6-5-2019

Vesicular glutamatergic transmission in noise-induced loss and repair of cochlear ribbon synapses

Kyunghee X. Kim
Washington University School of Medicine in St. Louis

Shelby Payne
Washington University School of Medicine in St. Louis

Aizhen Yang-Hood
Washington University School of Medicine in St. Louis

Song-Zhe Li
Washington University School of Medicine in St. Louis

Bethany Davis
Washington University School of Medicine in St. Louis

See next page for additional authors

Cellular/Molecular

Vesicular Glutamatergic Transmission in Noise-Induced Loss and Repair of Cochlear Ribbon Synapses

Kyunghee X. Kim,[1]* Shelby Payne,[1]* Aizhen Yang-Hood,[1] Song-Zhe Li,[1] Bethany Davis,[1,2] Jason Carlquist,[1] Babak V-Ghaffari,[1] Jay A. Gantz,[1] Dorina Kallogjeri,[1] James A.J. Fitzpatrick,[3] Kevin K. Ohlemiller,[1] Keiko Hirose,[1] and Mark A. Rutherford[1]

[1]Department of Otolaryngology, Washington University School of Medicine, [2]Program in Audiology and Communication Sciences, Washington University School of Medicine, St. Louis, Missouri 63110, and [3]Washington University Center for Cellular Imaging, Department of Neuroscience, Department of Cell Biology and Physiology, Department of Biomedical Engineering, Washington University School of Medicine, St. Louis, Missouri 63110

Noise-induced excitotoxicity is thought to depend on glutamate. However, the excitotoxic mechanisms are unknown, and the necessity of glutamate for synapse loss or regeneration is unclear. Despite absence of glutamatergic transmission from cochlear inner hair cells in mice lacking the vesicular glutamate transporter-3 ($Vglut3^{KO}$), at 9–11 weeks, approximately half the number of synapses found in $Vglut3^{WT}$ were maintained as postsynaptic AMPA receptors juxtaposed with presynaptic ribbons and voltage-gated calcium channels ($Ca_V1.3$). Synapses were larger in $Vglut3^{KO}$ than $Vglut3^{WT}$. In $Vglut3^{WT}$ and $Vglut3^{+/-}$ mice, 8–16 kHz octave-band noise exposure at 100 dB sound pressure level caused a threshold shift (~40 dB) and a loss of synapses (>50%) at 24 h after exposure. Hearing threshold and synapse number partially recovered by 2 weeks after exposure as ribbons became larger, whereas recovery was significantly better in $Vglut3^{WT}$. Noise exposure at 94 dB sound pressure level caused auditory threshold shifts that fully recovered in 2 weeks, whereas suprathreshold hearing recovered faster in $Vglut3^{WT}$ than $Vglut3^{+/-}$. These results, from mice of both sexes, suggest that spontaneous repair of synapses after noise depends on the level of Vglut3 protein or the level of glutamate release during the recovery period. Noise-induced loss of presynaptic ribbons or postsynaptic AMPA receptors was not observed in $Vglut3^{KO}$, demonstrating its dependence on vesicular glutamate release. In $Vglut3^{WT}$ and $Vglut3^{+/-}$, noise exposure caused unpairing of presynaptic ribbons and presynaptic $Ca_V1.3$, but not in $Vglut3^{KO}$ where $Ca_V1.3$ remained clustered with ribbons at presynaptic active zones. These results suggest that, without glutamate release, noise-induced presynaptic Ca^{2+} influx was insufficient to disassemble the active zone. However, synapse volume increased by 2 weeks after exposure in $Vglut3^{KO}$, suggesting glutamate-independent mechanisms.

Key words: cochlea; excitotoxicity; glutamate; noise exposure; regeneration; synaptopathy

Significance Statement

Hearing depends on glutamatergic transmission mediated by Vglut3, but the role of glutamate in synapse loss and repair is unclear. Here, using mice of both sexes, we show that one copy of the *Vglut3* gene is sufficient for noise-induced threshold shift and loss of ribbon synapses, but both copies are required for normal recovery of hearing function and ribbon synapse number. Impairment of the recovery process in mice having only one functional copy suggests that glutamate release may promote synapse regeneration. At least one copy of the *Vglut3* gene is necessary for noise-induced synapse loss. Although the excitotoxic mechanism remains unknown, these findings are consistent with the presumption that glutamate is the key mediator of noise-induced synaptopathy.

Introduction

Glutamate is recognized as the afferent neurotransmitter between cochlear inner hair cells (IHCs) and auditory nerve fibers (ANFs) (Ruel et al., 2008; Seal et al., 2008; Akil et al., 2012). Excessive activation of AMPA-type glutamate receptors may be sufficient to initiate excitotoxic damage to ANF terminals, as demonstrated by application of AMPA to the cochlea. In phar-

Received Aug. 29, 2018; revised March 22, 2019; accepted March 25, 2019.

Author contributions: K.X.K., S.P., A.Y.-H., S.-Z.L., J.C., J.A.G., and M.A.R. performed research; K.X.K., S.P., B.D., J.C., J.A.G., D.K., and M.A.R. analyzed data; B.V.-G., J.A.G., J.A.J.F., and M.A.R. contributed unpublished reagents/analytic tools; K.K.O. and M.A.R. edited the paper; K.H. and M.A.R. designed research; M.A.R. wrote the first draft of the paper; M.A.R. wrote the paper.

This work was supported by National Institutes of Health/National Institute on Deafness and Other Communication Disorders T35DC008765 to B.D., National Institutes of Health/National Institute on Deafness and Other Communication Disorders R01DC011315 to K.H., and the Department of Otolaryngology at Washington University. The Washington University Center for Cellular Imaging is supported by Washington University School of Medicine, the Children's Discovery Institute of Washington University and St. Louis Children's Hospital (CDI-CORE-2015-505),

macological experiments and in response to sound overexposure, ANF postsynaptic terminals swell and burst, producing postsynaptic damage and vacuolization (Puel et al., 1994; Wang and Green, 2011). The excitotoxic mechanisms of glutamate in the organ of Corti are unknown and may involve Ca^{2+}-permeable AMPA receptors (Puel et al., 1998; Eybalin et al., 2004; Sebe et al., 2017). The question of whether excess synaptic glutamate release drives noise-induced synapse loss has not been directly tested with a genetic approach. Moreover, the mechanisms of hair-cell synapse repair are not fully understood. Neurotrophin-3 may enhance repair after noise exposure (Wan et al., 2014), but the role of glutamate is unclear.

In addition to glutamate release, sound overexposure may activate multiple damage pathways by releasing adenosine, aspartate, protons, and proinflammatory cytokines (Jäger et al., 1998; Peng et al., 2004; Wakabayashi et al., 2010; Kurabi et al., 2017). Upstream of glutamate release from the IHC, damage to the presynaptic active zone may involve Ca^{2+} influx through voltage-gated Ca^{2+} channels at the IHC ribbon synapses. Glutamate is concentrated into synaptic vesicles in IHCs by vesicular glutamate transporter type 3 (Vglut3), pathogenic variants of which cause nonsyndromic deafness DFNA25 in humans (Greene et al., 2001; Thirlwall et al., 2003; Ruel et al., 2008). To isolate the roles of Vglut3 in noise damage and repair in the inner ear, we studied mice having 0, 1, or 2 functional copies of the *Vglut3* gene (*SLC17A8*).

Vglut3^{WT} and heterozygous (*Vglut3*$^{+/-}$) mice have similar hearing thresholds measured by auditory brainstem response (ABR), suggesting that one copy of *Vglut3* is sufficient for hearing low-level sounds. *Vglut3*^{KO} mice are profoundly deaf but have no obvious functional vestibular deficit and otherwise develop relatively normally. In *Vglut3*^{KO}, the outer hair cells, responsible for cochlear amplification, still transduce sound and generate distortion product otoacoustic emissions (DPOAEs). The IHCs of *Vglut3*^{KO} mice form ribbon synapses with ANFs; they develop a mature complement of basolateral ion channels, including $Ca_V1.3$; and they exocytose the contents of synaptic vesicles upon depolarization, like *Vglut3*^{WT}, but in *Vglut3*^{KO} the synaptic vesicles lack glutamate (Ruel et al., 2008; Seal et al., 2008).

Here, to address the roles of vesicular glutamate in the mechanisms of synapse loss and regeneration after overexposure to sound, we assessed hearing function and synaptic anatomy in *Vglut3* mice on C57BL/6J background at 0 h, 24 h, 14 d, and 28 d after noise exposure. Our findings show that glutamate is required, and that presynaptic Ca^{2+} influx alone is likely insufficient, for loss of synapse number. Interestingly, noise trauma to *Vglut3*^{KO} did induce changes in ribbon synapse morphology, suggesting glutamate-independent mechanisms.

After noise trauma in *Vglut3*^{WT} and *Vglut3*$^{+/-}$ mice on C57BL/6J background, we found an immediate reduction of synapse number per IHC. This was followed by partial recovery of synapse number, contrasting with results in CBA/CaJ mice showing no recovery (Kujawa and Liberman, 2009; Liberman et al., 2015), but similar to findings in guinea pig showing partial recovery after noise trauma (Shi et al., 2013). Following noise trauma, recovery of hearing function and synapse number was more complete in *Vglut3*^{WT} than *Vglut3*$^{+/-}$, suggesting a role for Vglut3 and glutamate transmission in ribbon synapse repair and recovery of hearing function.

Materials and Methods

Animals. Mice were used in accordance with protocols approved by the Animal Studies Committee of Washington University in St. Louis. *Vglut3* mice (*Slc17a8*^{tm1Edw}) on C57BL/6J background were obtained from The Jackson Laboratory (RRID:IMSR_JAX:016931). We used mice of either sex in similar proportions aged 2–3 months (normative studies) or 2–9 months (to study age-related hearing loss on C57BL/6J background).

Acoustic overexposure. We exposed awake unrestrained mice to 2 h of 8–16 kHz octave band noise at a sound pressure level (SPL) of 94 or 100 dB (Hirose et al., 2005), known to cause swelling in the peripheral terminals of ANFs in the basal (high-frequency) half of the cochlea. Cochlear responses to threshold-level tones define the tonotopic map (Müller et al., 2005). As SPL increases, the region of excitation broadens, and the focal region of excitation shifts toward mid-frequency regions corresponding to the center of the threshold audiogram (Lee et al., 2019). As 8–16 kHz is a relatively low-frequency range for mouse, with increasing SPL, the focal region broadens and shifts from more apical cochlear regions toward higher-frequency regions in the cochlear base (see Fig. 1). Mice were placed in individual cages on a suspended shelf in a custom-made acrylic chamber in which no two sides were parallel. The sound stimulus was produced by an RX6 processor (Tucker-Davis Technologies), filtered (Frequency Devices), amplified (Crown 75A power amplifier), and delivered to the acrylic chamber via a speaker horn (JBL). The SPL was measured through a 1/4-inch free-field microphone (ACO Pacific) calibrated to a 124-dB pistonphone (Bruel and Kjaer). Before the experimental noise exposure, four quadrants of the chamber were sampled with the 1/4-inch microphone, and sound pressure was confirmed to vary by no more than 0.5 dB across these measurement positions.

ABR and distortion product otoacoustic emissions. Hearing was assessed 3 d before acoustic overexposure and reassessed at 24 h after exposure (1 d group), 14 d after exposure (2 week group), and 28 d after exposure (4 week group). The ABR is a sound-evoked potential reflecting activation of the ANFs by the IHCs (wave I), and subsequent activation of the ascending auditory pathways (waves II-V). Responses were recorded from subcutaneous electrodes located at the vertex (active electrode) and behind the right pinna (reference electrode), with ground electrode placed on the back, under ketamine (100 mg/kg)/xylazine (20 mg/kg) anesthesia, using a sampling frequency of 25 kHz. ABR thresholds in response to tone pips at frequencies presented in half-octave intervals (5.6, 8, 11.2, 16, 22.6, 32, 45.2, and 64 kHz) were determined using 5 ms tone pips (including 0.5 ms cosine^2 rise/fall) at a repetition rate of 40 s^{-1}. The responses were amplified (×10,000), filtered (100 Hz to 3 kHz), and averaged using custom computer software (System 3; Tucker-Davis Technologies). Stimuli were presented in 5 dB steps from 15 dB to 100 dB SPL in ascending order to the right ear. At each level, 1024 responses were averaged, with stimulus polarity alternated. Response waveforms were rejected if the peak-to-peak voltage exceeded 15 μV. Threshold was determined by a single observer, who noted the lowest sound level at which a recognizable waveform was present. Waveforms were confirmed as auditory-evoked responses by their increasing amplitude and decreasing latency with increasing SPL. If hearing threshold was not detected at 100 dB SPL, the threshold value was assigned as >100 dB. For wave I measurements, ABRs were evoked with tone pips presented at a rate of 21 s^{-1} and measured using Tucker-Davis Technologies hardware in conjunction with BiosigRZ software (Tucker-Davis Technologies). Stimuli were presented in 5 dB steps in descending order to the right ear. Responses to 500 stimulus presentations at each level were used to construct average ABR waveforms. ABR wave I amplitudes were quantified offline at 8,

the Foundation for Barnes-Jewish Hospital (3770), and National Institutes of Health/OD S10OD021629 to J.A.J.F. The research was funded by an International Project Grant from Action on Hearing Loss, a Small Grant from the McDonnell Center for Cellular and Molecular Neurobiology, and National Institutes of Health/National Institute on Deafness and Other Communication Disorders R01DC014712 to M.A.R. We thank Tejbeer Kaur, Mark Warchol, Maria Rubio, and the Washington University Auditory/Vestibular Neuroscience Group for helpful discussion; and Lavinia Sheets for comments on the manuscript.

The authors declare no competing financial interests.

*K.X.K. and S.P. contributed equally to this work.

Correspondence should be addressed to Mark A. Rutherford at RutherfordM@ent.wustl.edu.

K.X. Kim's present address: Department of Otolaryngology-Head and Neck Surgery, University of California, San Francisco, CA 94158.

https://doi.org/10.1523/JNEUROSCI.2228-18.2019

22.6, and 45.2 kHz as the difference between the prestimulus baseline and the first positive peak. To assess the status of the cochlear outer hair cells, we measured DPOAEs with a microphone in the ear canal. DPOAEs were recorded from the right ear using Emav software (S. Neely, Boys Town National Research Hospital) in conjunction with Tucker-Davis Technologies and custom hardware, using a sampling rate of 192 kHz. We measured cochlear emissions at $2f_1$-f_2, with f_2 frequencies from 5 to 40 kHz (total of 25 tone pairs, 8 per octave). The f_1/f_2 ratio was 1.22. Tone levels were set to 75 dB SPL (L_1) and 65 dB SPL (L_2). The mean level of the DPOAE across frequencies per mouse was used to calculate group means as a function of time after exposure in Figure 9*C–E*. The frequency-specific level of the DPOAE was used to calculate group means as a function of f_2 in Figure 9*A,B*.

Immunohistofluorescence, confocal microscopy, synapse counts, volume, and intensity measurements. Synapse loss and recovery after 100 dB SPL noise exposure were quantified on left cochleae immediately after the terminal ABR/DP assessment on right cochleae. Briefly, after cardiac perfusion with 4% PFA, for whole-mount preparations, organ of Corti and spiral ganglion were isolated from the cochlea in three pieces containing the apical, middle, and basal thirds. Antibodies: CtBP2 mouse (BD Biosciences; RRID:AB_399431), $Ca_V1.3$ rabbit (Alomone Labs; RRID:AB_2039775), GluA3 goat (Santa Cruz Biotechnology; RRID: AB_2113895), and Myosin7a rabbit (Proteus Biosciences; RRID: AB_2314838) primary antibodies were used with species-appropriate secondary antibodies conjugated to AlexaFluor (Invitrogen) fluorophores excited by 488, 555, or 647 nm light in triple-labeled samples as previously described (Jing et al., 2013; Sebe et al., 2017). Samples were batch processed using the same reagent solutions in six cohorts, each including exposed and unexposed *Vglut3*^{WT}, *Vglut3*$^{+/-}$, and *Vglut3*^{KO} mice. For synapse counts, intensity, and volume measurements, confocal stacks were collected without saturation of pixel intensity and sampled with a *z* step of 0.38 μm and with pixel size of 100 nm in *x* and *y*, on an LSM 700 with a 63 × 1.4 NA oil objective lens (Carl Zeiss). From the left cochlea of 34 mice, we collected 2 or 3 images at each of 3 cochlear regions centered near tonotopic characteristic frequencies of 9, 22.5, and 44.5 kHz (Müller et al., 2005). The numbers of IHCs and synapses were counted manually using the maximum-intensity projection (ImageJ software, National Institutes of Health) and the individual optical sections (Zen software, Carl Zeiss) to calculate the mean number of synapses per IHC in each image. For each group, grand means were calculated across images. Synapses were identified as juxtaposed pairs of presynaptic ribbons (labeled with anti-CtBP2) and postsynaptic AMPA-type glutamate receptor puncta (labeled with anti-GluA3), which appear to partly overlap at confocal resolution (Rutherford, 2015). CtBP2 puncta were identified as unpaired ribbons when they appeared to be in the IHC cytoplasm, completely overlapping with Myosin7a but without juxtaposed GluA3. For unpaired ribbons, we did not attempt to distinguish membrane-anchored from unanchored. GluA3 puncta were identified as unpaired "ribbonless" synapses when they lacked juxtaposed CtBP2 but appeared to be on the surface of the Myosin7a-labeled IHC. For unpaired GluA3, we distinguished ribbonless synapses on the cell surface from GluA3 puncta that may have been internalized in the IHC cytoplasm by excluding those puncta that appeared to completely overlap with Myosin7a in three dimensions. Synapses were quantified from mice killed 2–3 d before exposure, 1 d after exposure, or 2 weeks after exposure. The volumes of paired presynaptic ribbons and postsynaptic GluA3 were measured in Imaris software (Bitplane) by segmenting the synaptic elements from the 3D image as "surface" objects, using identical settings for each image stack, including the "local contrast background subtraction" algorithm for calculating threshold. This automatic thresholding algorithm compensates for differences in overall luminance between stacks and avoids potential subjective bias of setting a user-defined arbitrary threshold value. In some experiments, anti-Myosin7a was replaced with anti-$Ca_V1.3$ to assess presynaptic Ca^{2+} channels in unexposed ears or at 0 h after noise exposure. Intensities of synaptic ribbons, voltage-gated Ca^{2+} channels, and AMPA receptors were measured in Imaris software as the sum of pixel intensities within surface objects (Sebe et al., 2017). For display only, some images were acquired on an LSM 880 (Carl Zeiss) with Airyscan processing using a 100× 1.5 NA oil objective lens, a *z* step of 0.15 μm, and a pixel size of 40 nm in *x* and *y*.

Experimental design and statistical analysis. Data were tested for normality with the Shapiro–Wilk test or assumed to be not normally distributed due to sample size. Parametric or nonparametric tests were applied as appropriate. All statistical values are presented as mean ± SD; mixed-model ANOVA: analysis with autoregressive covariance structure and individual subjects as a random factor was implemented using PROC MIXED procedure (Littell et al., 1998). The mixed-model approach is particularly useful for repeated measures on subjects over time (longitudinal studies) because it makes maximum use of the data available at any assessment time (deals with missing data). Here, it was used to investigate differences between animal groups and changes within groups over subsequent assessment times after noise exposure; exact *p* values are given. Dunnett's test was used for pairwise comparisons of multiple experimental groups to one control group; the family-wise error rate was kept below α. Planned bivariate analyses were used for comparisons between groups at specific probe frequency or level, or cochlear location. Wilcoxon rank-sum test was used for comparisons between two groups within assessment times at specific probe frequencies or levels; exact *p* values are given. To compare two samples of synapse volumes, we used the Kolmogorov–Smirnov test; exact *p* values are given; effect size was estimated as the absolute value of the difference between medians divided by the pooled SD. *N* is the number of animals or cochleae, as indicated in each figure legend or table. All statistical tests were two-sided and evaluated at the α level of 0.05 in SAS 9.4 (SAS; RRID:SCR_008567), Excel (Microsoft; RRID:SCR_016137), or IGOR Pro 7 (Wavemetrics; RRID:SCR_000325). For multiple comparisons with Student's *t* test, the α level was adjusted with the Bonferroni correction and the exact *p* value or range is reported. Graphs were plotted in IGOR.

Results

Cochlear function in *Vglut3* mice before and after 100 dB exposure

The ABR is a measure of neuronal activity of the ascending auditory pathway. It depends on synchronous activation of ANFs by synaptic release of glutamate from IHCs at the onset of sound. The minimum sound level required to evoke an ABR at a given frequency relates closely to the threshold of perception defined by the behavioral audiogram in mice and human (Elberling and Don, 1987; Longenecker et al., 2016). ABR thresholds in unexposed *Vglut3*^{WT} and *Vglut3*$^{+/-}$ mice at 9–11 weeks of age were not significantly different from each other at any of the 8 test frequencies (Fig. 1*A*). In contrast, *Vglut3*^{KO} mice typically showed no ABR (Fig. 1*A*), although some mice exhibited very small responses to high-SPL tone bursts (Fig. 1*A*; see 7*C*).

In *Vglut3*^{WT} and *Vglut3*$^{+/-}$ mice, 2 h of 8–16 kHz noise at 100 dB SPL caused a threshold shift at 1 d that recovered incompletely by 2 weeks after exposure. ABR thresholds measured 1 d after exposure were significantly elevated relative to unexposed mice at test frequencies between 11.2 and 45.2 kHz, reaching a maximum shift of ~50 dB at 16 kHz (Fig. 1*B*). Although ABR thresholds of *Vglut3*^{WT} and *Vglut3*$^{+/-}$ mice were not significantly different from each other for any test frequency at 1 d after exposure, by 2 weeks after exposure, recovery of ABR threshold was significantly better in *Vglut3*^{WT} than *Vglut3*$^{+/-}$ for three mid-frequency probe tones: 11.2, 16, and 32 kHz (Fig. 1*C*; Table 1). Next, we looked at the ribbon synapses between IHCs and ANFs, where the electrical signal of the ABR is initiated.

Ribbon synapse number in *Vglut3* mice before and after 100 dB exposure

Presynaptic ribbons and postsynaptic AMPA receptors are juxtaposed on either side of the IHC-ANF synaptic cleft. Figure 2 compares ribbon synapses from a mid-basal cochlear location in

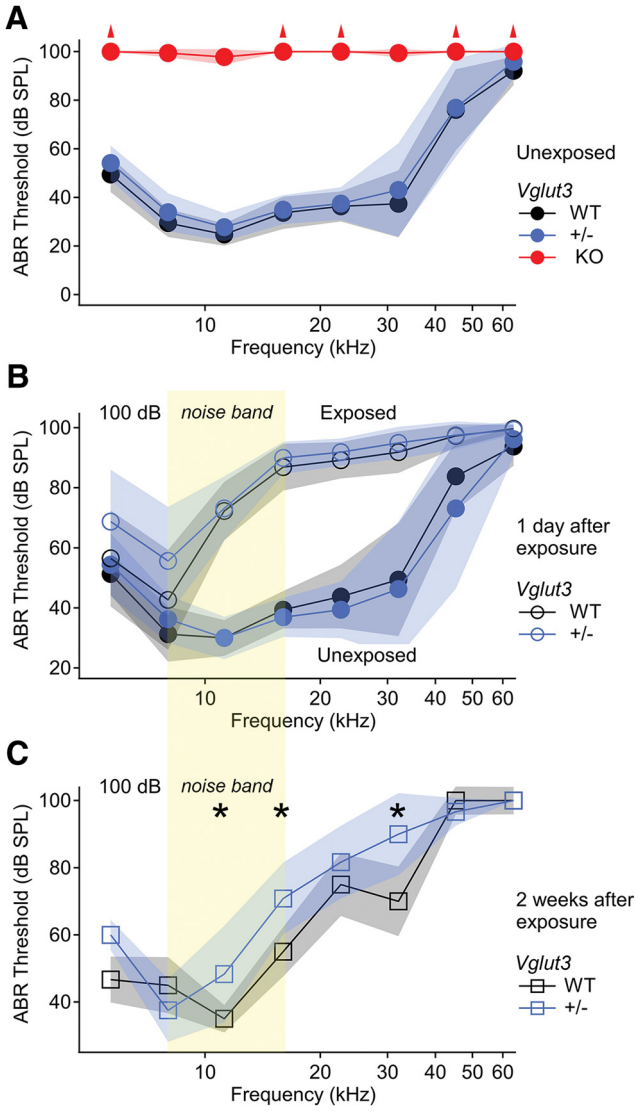

Figure 1. Better recovery of ABR thresholds in $Vglut3^{WT}$ than $Vglut3^{+/-}$ after 100 dB exposure. ***A***, ABR thresholds (mean ± SD) for unexposed mice aged 9–11 weeks. $Vglut3^{KO}$ are profoundly deaf. Red arrowheads indicate thresholds > 100 dB SPL. Unexposed $Vglut3^{WT}$ and $Vglut3^{+/-}$ had similar thresholds. ***B***, Comparison of ABR thresholds before (unexposed, filled circles) and 1 d after exposure (exposed, open circles) to 2 h of 100 dB SPL, 8–16 kHz octave-band noise. Yellow rectangle indicates frequency band of noise. Threshold shifts exceeded 40 dB in the mid-frequencies for $Vglut3^{WT}$ and $Vglut3^{+/-}$ mice. Threshold shifts occur for test frequencies within the noise band and also for higher frequencies that probe more basal cochlear locations. ***C***, Two weeks after exposure (open squares), ABR thresholds had recovered better in $Vglut3^{WT}$ than $Vglut3^{+/-}$. $N = 6–19$ animals per group. *Frequencies for which thresholds of $Vglut3^{WT}$ are significantly lower than $Vglut3^{+/-}$ ($p < 0.05$).

Table 1. ABR thresholds (dB SPL, mean ± SD) for test frequencies showing significant differences between $Vglut3^{WT}$ and $Vglut3^{+/-}$ 2 weeks after 100 dB exposure[a]

	Tone frequency (kHz)		
	11.2	16	32
$Vglut3^{WT}$	33.3 ± 4.1	50.8 ± 7.4	72.5 ± 10.4
$Vglut3^{+/-}$	48.3 ± 14.4	70.9 ± 10.7	90.0 ± 12.3
p (Wilcoxon rank sum test)	0.048	0.012	0.039

[a]See also Figure 1.

10-week-old unexposed $Vglut3^{WT}$ and unexposed $Vglut3^{KO}$ IHCs. $Vglut3^{+/-}$ (data not shown) and $Vglut3^{WT}$ cochleae (Fig. 2*A*) had ~15 ribbon synapses per IHC, populating the basolateral membrane extending ~10 μm below the IHC nucleus. In contrast, in the basal half of the cochlear spiral of $Vglut3^{KO}$ mice, we noted truncation of IHC basolateral membranes (Fig. 2*B*), which we also observed in plastic mid-modiolar sections (data not shown). Unexposed $Vglut3^{KO}$ had fewer ribbon synapses per IHC, and they appeared to be larger in size than unexposed $Vglut3^{+/-}$ or $Vglut3^{WT}$, as quantified below.

Ribbons without paired AMPA receptors, or vice versa, were rare in unexposed mice (Fig. 3*A*). Based primarily on studies in CBA/CaJ ^{WT} mice, 2 h of 100 dB SPL 8–16 kHz noise exposure is expected to cause swelling of the ANF postsynaptic terminals and disintegration of the corresponding presynaptic and postsynaptic elements on IHCs in the (high-frequency) basal half of the cochlea (Kujawa and Liberman, 2009). One day after the 100 dB SPL noise exposure in $Vglut3^{WT}$ and $Vglut3^{+/-}$ cochleae, there were many unpaired synaptic puncta, and few paired synapses that persisted (Fig. 3*B*). By 2 weeks after exposure, many synaptic puncta had apparently repaired (Fig. 3*C*). Unpaired synaptic puncta were rarely observed 2 weeks after exposure, but they remained in greater proportion than in unexposed animals. While Figure 2 illustrates the phenomenon in $Vglut3^{WT}$ mice, similar observations were made in $Vglut3^{+/-}$.

We quantified hair-cell synapse loss and repair by calculating the mean number of paired synapses per IHC in three cochlear regions. Unexposed $Vglut3^{WT}$ and $Vglut3^{+/-}$ mice had more synapses per IHC than $Vglut3^{KO}$ in all three regions (Fig. 4*A–C*). The ABR threshold shift for middle and high frequencies at 1 d after exposure (Fig. 1*B*) was accompanied by ≥50% loss of synapse number in $Vglut3^{WT}$ and $Vglut3^{+/-}$ cochleae in the midcochlear and basal regions corresponding, respectively, to characteristic frequencies centered at ~22.5 and 44.5 kHz (Fig. 4*B*, *C*). Relative to unexposed controls, on average, there were 9.5 fewer synapses per IHC in the $Vglut3^{WT}$ midcochlea and 9.6 fewer in the $Vglut3^{+/-}$ midcochlea at 1 d after exposure (Table 2). In the basal cochlea, noise-induced synapse loss per IHC was more extreme: 11.1 in $Vglut3^{WT}$ and 12.0 in $Vglut3^{+/-}$, on average.

At 2 weeks after exposure, we observed incomplete recovery of synapse numbers in $Vglut3^{WT}$ and $Vglut3^{+/-}$ IHCs at the 22.5 and 44.5 kHz locations (Fig. 4*B*, *C*). Although synapse loss was similar at 1 d after exposure, recovery of synapse number was greater in $Vglut3^{WT}$ than $Vglut3^{+/-}$ by 2 weeks after exposure. On average, $Vglut3^{WT}$ recovered 5.5 synapses per IHC at the 22.5 kHz location and 6.3 at the 44.5 kHz location, whereas $Vglut3^{+/-}$ cochleae recovered only 3.1 and 2.5 synapses per IHC, respectively (Table 2). Results of the mixed-model ANOVA revealed a significant difference between $Vglut3^{WT}$ and $Vglut3^{+/-}$ in number of synapses per IHC at 2 weeks after exposure ($p = 0.0089$). Synapses per IHC in the apical region (~9 kHz) of $Vglut3^{WT}$, $Vglut3^{+/-}$, or $Vglut3^{KO}$ cochleae appeared unchanged in response to the 100 dB SPL exposure (Fig. 4*A*). In mid-frequency and high-frequency regions in $Vglut3^{KO}$, unlike in $Vglut3^{WT}$ or $Vglut3^{+/-}$, noise exposure did not result in loss of synapse number (Fig. 4*B*, *C*; Table 2).

We also counted the numbers of unpaired synaptic puncta before and after the 100 dB SPL noise exposure (Table 3). In unexposed animals, the mean number of unpaired puncta per IHC was <1. In $Vglut3^{KO}$ cochleae and in the apical (low-frequency) regions of $Vglut3^{WT}$ and $Vglut3^{+/-}$ cochleae, there remained <1 unpaired punctum per IHC at 1 d and 2 weeks after noise exposure. In contrast, in the mid-cochlear and basal regions

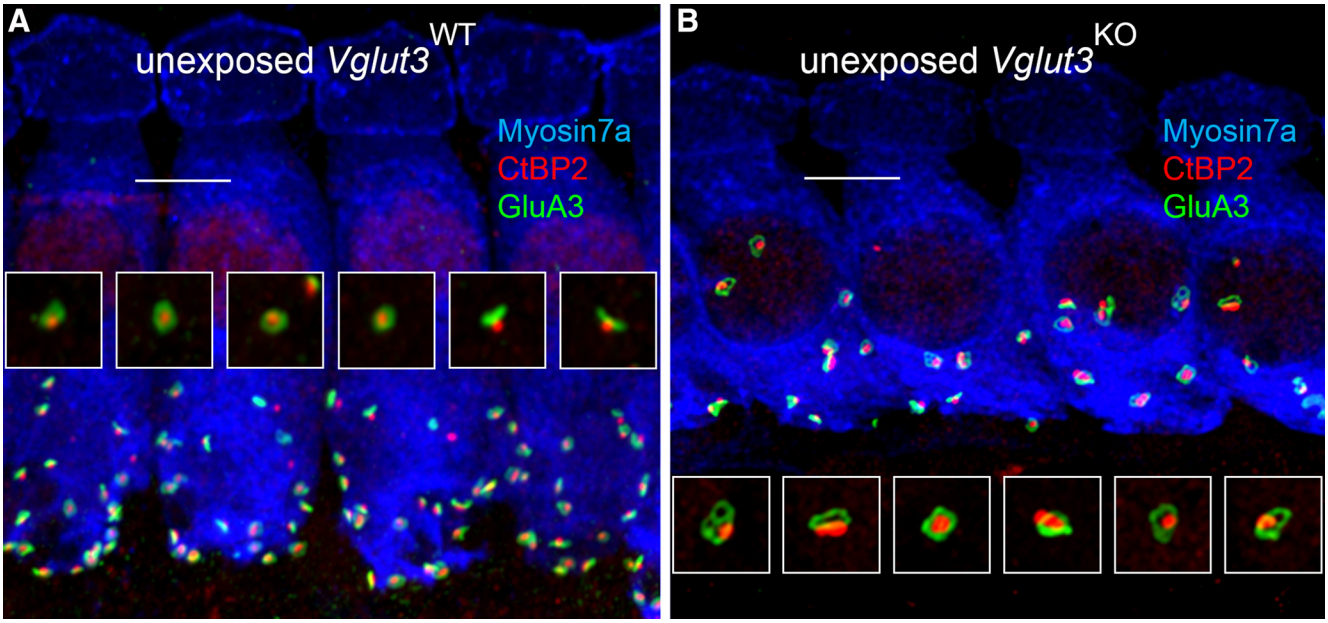

Figure 2. Synapses are fewer in number in unexposed *Vglut3*^{KO} mice. ***A***, ***B***, Confocal images of 10-week-old unexposed *Vglut3*^{WT} (***A***) and *Vglut3*^{KO} (***B***) IHCs labeled with anti-Myosin7a (blue), anti-CtBP2 (red), and anti-GluA3 (green). Imaged with LSM 880 Airyscan. Scale bars, 5 μm. Boxes are 3 $\times$ 3 μm.

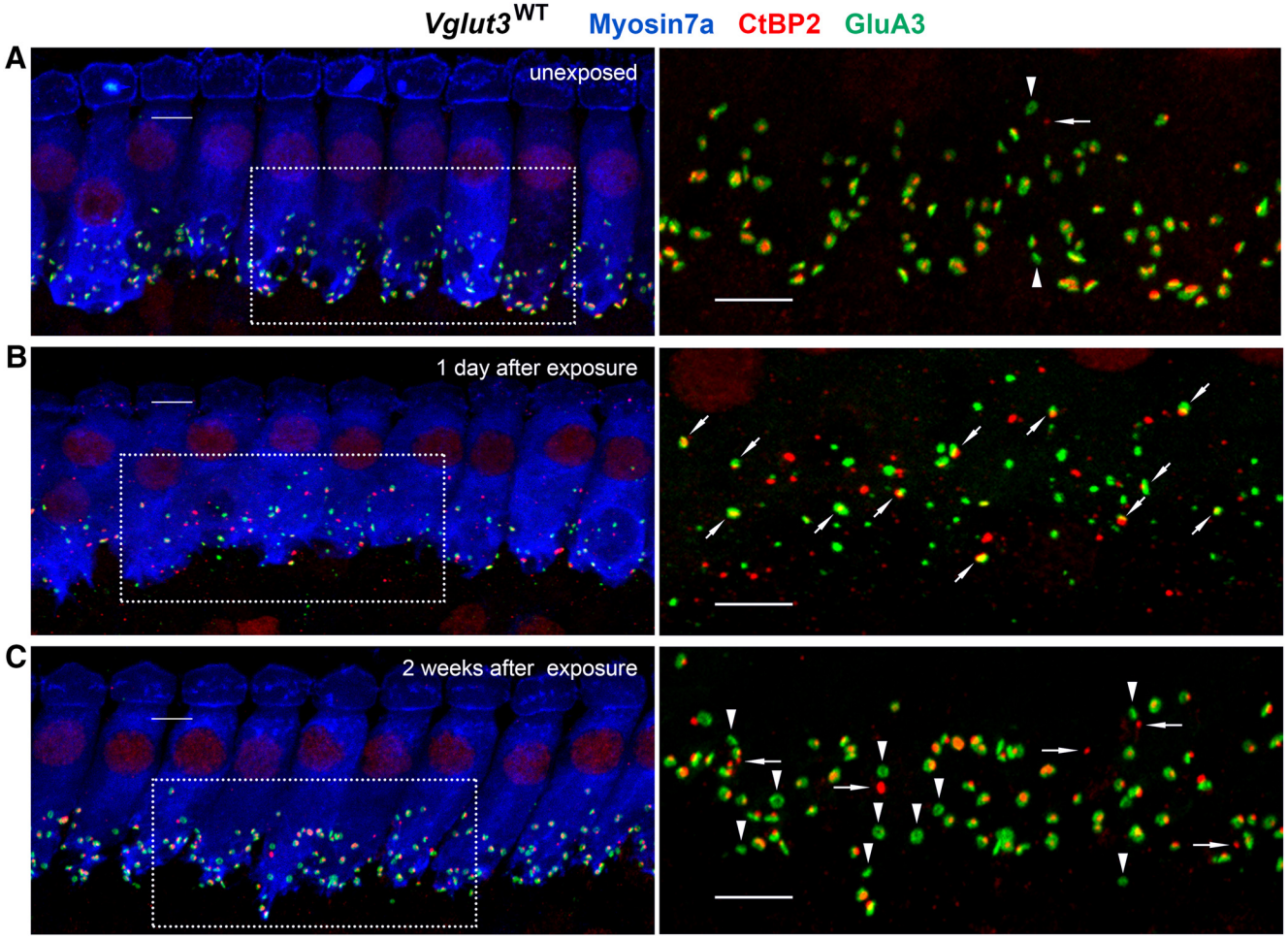

Figure 3. Synapses are lost and repaired following 100 dB noise exposure in *Vglut3*^{WT}. Confocal images of 10-week-old *Vglut3*^{WT}. Left, IHCs are labeled with anti-Myosin7a, presynaptic ribbons with anti-CtBP2, and postsynaptic AMPA receptors with anti-GluA3. Right, White rectangular regions are enlarged. Midcochlear location, ~22.5 kHz. ***A***, Unexposed cochleae. Horizontal arrow indicates a lone ribbon. Vertical arrowheads point to ribbonless synapses. ***B***, One day after exposure. Diagonal arrows indicate synapses that remain paired. ***C***, Two weeks after exposure. Horizontal arrows indicate lone ribbons. Vertical arrowheads point to ribbonless synapses. Similar observations were made in *Vglut3*$^{+/-}$ (data not shown). Imaged with LSM 700. Scale bars, 5 μm.

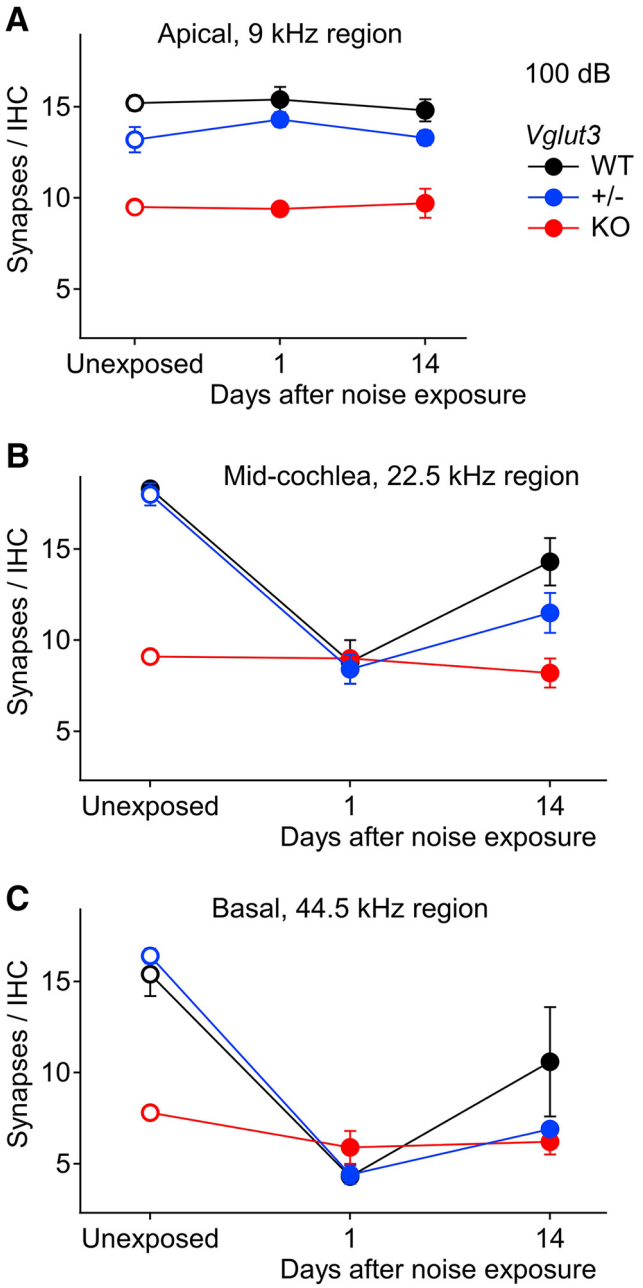

Figure 4. No loss of synapse number in *Vglut3*^{KO}, and greater recovery of synapse number in *Vglut3*^{WT} than *Vglut3*$^{+/-}$ after 100 dB exposure. ***A–C***, Paired synapses (mean ± SD) per IHC in unexposed mice (open circles) and as a function of time after exposure (filled circles) for each genotype at the three cochlear locations: ***A***, apical; ***B***, mid-cochlea; ***C***, basal. For 9 groups (3 genotypes × 3 assessment times): total 34 mice, $N = 3–5$ per group; 10–12 complete IHCs per image; 205 images (73 apical, 71 mid-cochlear, 61 basal); 5–11 cochleae per group.

of *Vglut3*^{WT} and *Vglut3*$^{+/-}$, the numbers of unpaired GluA3 puncta and unpaired ribbons changed after noise exposure, showing similar trends. Loss of paired puncta at 1 d after exposure was accompanied by an increase in unpaired puncta (Tables 2, 3). By 2 weeks after exposure, the numbers of unpaired puncta were reduced relative to 1 d after exposure but still greater than in unexposed ears. Unpaired GluA3 puncta were in greater abundance than unpaired ribbons in 24 of 27 cases (3 genotypes × 3 cochlear locations × 3 assessment times). After noise exposure, on average, the sum of paired synapses and unpaired ribbon or AMPA receptor puncta was smaller than the number of paired puncta in unexposed mice, suggesting that some unpaired synaptic puncta had been eliminated from the ROI.

Table 2. Paired synapses (mean ± SD) per IHC in unexposed, 1 d, or 2 weeks after 100 dB SPL exposure in *Vglut3*^{WT}, *Vglut3*$^{+/-}$, and *Vglut3*^{KO} in apical, middle, and basal cochlea[a]

		Unexposed	1 d	2 weeks
Tonotopic region (kHz)				
Apical (9)	*Vglut3*^{WT}	15.2 ± 0.4	15.4 ± 0.7	14.8 ± 0.6
	Vglut3$^{+/-}$	13.2 ± 0.7	14.3 ± 0.4	13.3 ± 0.4
	Vglut3^{KO}	9.5 ± 0.2	9.4 ± 0.3	9.7 ± 0.8
Middle (22.5)	*Vglut3*^{WT}	18.3 ± 0.2	8.8 ± 1.2	14.3 ± 1.3
	Vglut3$^{+/-}$	18.0 ± 0.6	8.4 ± 0.8	11.5 ± 1.1
	Vglut3^{KO}	9.1 ± 0.2	9.0 ± 0.2	8.2 ± 0.8
Basal (44.5)	*Vglut3*^{WT}	15.4 ± 1.2	4.3 ± 0.3	10.6 ± 3.0
	Vglut3$^{+/-}$	16.4 ± 0.4	4.4 ± 0.5	6.9 ± 0.3
	Vglut3^{KO}	7.8 ± 0.2	5.9 ± 0.9	6.2 ± 0.7

[a]See also Figure 4.

Presynaptic ribbon and postsynaptic AMPA receptor volumes before and after 100 dB exposure

Exposure to excitotoxic noise resulted in synapse loss in *Vglut3*^{WT} and *Vglut3*$^{+/-}$, but not in *Vglut3*^{KO} (Fig. 4; Table 2). Thus, synaptic glutamate release seems to be required for outright synapse loss, but presynaptic Ca^{2+} influx or nonglutamatergic transmission may have measurable effects in the absence of glutamate in *Vglut3*^{KO}. In addition, noise exposure may have effects on the properties of surviving or regenerated synapses in *Vglut3*^{WT} and *Vglut3*$^{+/-}$. Therefore, we assessed the effects of noise and *Vglut3* copy number on synapse morphology by comparing presynaptic ribbon volume and postsynaptic GluA3 volume among mid-cochlear synapses in *Vglut3*^{WT}, *Vglut3*$^{+/-}$, and *Vglut3*^{KO} IHCs before and 2 weeks after the 100 dB noise exposure. The distributions of synapse volumes for the 12 groups (3 genotypes × 2 conditions × CtBP2 or GluA3) were all non-normal and positively skewed (Fig. 5; Table 4).

For presynaptic ribbons, labeled with anti-CtBP2, the distributions of volumes in *Vglut3*^{KO} were larger, and significantly different from those of *Vglut3*$^{+/-}$ or *Vglut3*^{WT} before and 2 weeks after noise exposure (Fig. 5, left). In contrast, *Vglut3*^{WT} and *Vglut3*$^{+/-}$ ribbon volume distributions were not significantly different from each other before or after noise. Moreover, the 100 dB noise exposure resulted in significant changes to the ribbon volume distributions relative to unexposed (Table 4). Ribbons were larger 2 weeks after exposure in *Vglut3*^{WT}, *Vglut3*$^{+/-}$, and *Vglut3*^{KO}. Therefore, noise exposure or loss of both *Vglut3* genes was associated with larger ribbon volumes, suggesting a greater number of CtBP2/Ribeye molecules per synapse.

For postsynaptic AMPA receptors labeled with anti-GluA3, as in the case for ribbons, the distributions of volumes in *Vglut3*^{KO} were larger and significantly different from those of *Vglut3*$^{+/-}$ or *Vglut3*^{WT} before and 2 weeks after noise exposure (Table 4). Also, the mean and median GluA3 volumes of the *Vglut3*$^{+/-}$ synapses were intermediate, between the larger *Vglut3*^{KO} and the smaller *Vglut3*^{WT} volumes, before and 2 weeks after noise exposure (Fig. 5, right). Thus, fewer copies of the *Vglut3* gene were associated with larger GluA3 volumes, suggesting a greater number of AMPA receptors per synapse. Moreover, 2 weeks after 100 dB noise exposure, the distributions of GluA3 volumes were larger and significantly different from unexposed GluA3 volumes in *Vglut3*$^{+/-}$ and *Vglut3*^{KO}, but not in *Vglut3*^{WT}.

In summary, except for GluA3 puncta in *Vglut3*^{WT}, the general effect of 100 dB noise exposure on synapse volume after 2

Table 3. Unpaired ribbons and GluA3 puncta (mean ± SD) per IHC in unexposed, 1 d, or 2 weeks after 100 dB SPL exposure in *Vglut3*^{WT}, *Vglut3*$^{+/-}$, and *Vglut3*^{KO} in apical, middle, and basal cochlear regions[a]

		Ribbons			GluA3		
		Unexposed	1 d	2 weeks	Unexposed	1 d	2 weeks
Tonotopic region (kHz)							
Apical (9)	*Vglut3*^{WT}	0.2 ± 0.1	0.2 ± 0.0	0.3 ± 0.0	0.4 ± 0.1	0.3 ± 0.1	0.2 ± 0.1
	Vglut3$^{+/-}$	0.2 ± 0.1	0.3 ± 0.1	0.5 ± 0.1	0.4 ± 0.1	0.5 ± 0.1	0.5 ± 0.2
	Vglut3^{KO}	0.4 ± 0.1	0.4 ± 0.1	0.4 ± 0.1	0.4 ± 0.0	0.7 ± 0.1	0.4 ± 0.1
Middle (22.5)	*Vglut3*^{WT}	0.3 ± 0.1	1.8 ± 0.4	0.8 ± 0.1	0.5 ± 0.1	3.2 ± 0.6	1.9 ± 0.6
	Vglut3$^{+/-}$	0.2 ± 0.1	2.2 ± 0.4	0.8 ± 0.1	0.2 ± 0.1	4.7 ± 0.9	1.6 ± 0.3
	Vglut3^{KO}	0.5 ± 0.0	0.6 ± 0.1	0.6 ± 0.2	0.4 ± 0.1	0.8 ± 0.2	0.9 ± 0.2
Basal (44.5)	*Vglut3*^{WT}	0.3 ± 0.1	2.5 ± 0.3	0.4 ± 0.0	0.7 ± 0.1	3.1 ± 0.3	1.6 ± 0.2
	Vglut3$^{+/-}$	0.5 ± 0.3	2.8 ± 0.3	1.4 ± 0.3	0.5 ± 0.3	4.4 ± 0.6	2.8 ± 0.2
	Vglut3^{KO}	0.3 ± 0.1	0.6 ± 0.2	0.7 ± 0.2	0.4 ± 0.1	0.6 ± 0.2	0.6 ± 0.2

[a]See also Figure 4.

weeks relative to unexposed controls was ribbon and GluA3 enlargement (Fig. 5; Table 4). Greater synapse volume in unexposed *Vglut3*^{KO} relative to unexposed *Vglut3*^{WT} or *Vglut3*$^{+/-}$ suggests glutamate-dependent maintenance of synapse size. In addition, greater volumes of presynaptic ribbons and postsynaptic GluA3 2 weeks after exposure in *Vglut3*^{KO} suggests noise-induced glutamate-independent mechanisms of changes in synapse morphology.

Presynaptic $Ca_V1.3$ before and after noise exposure

Although *Vglut3*^{KO} mice are profoundly deaf, *Vglut3*^{KO} IHCs support fast Ca^{2+}-dependent exocytosis as measured by depolarization-evoked membrane capacitance increases (Ruel et al., 2008). In *Vglut3*^{WT} mice, exocytosis is thought to occur predominantly at the ribbon synapses, where voltage-gated Ca^{2+} channels ($Ca_V1.3$) cluster in the presynaptic membrane (Martinez-Dunst et al., 1997; Rutherford, 2015; Ohn et al., 2016). In *Vglut3*^{KO} IHCs, whole-cell voltage-gated Ca^{2+} currents were significantly larger than those in *Vglut3*^{WT} IHCs (Seal et al., 2008; Ruel et al., 2008). However, the subcellular localization of $Ca_V1.3$ in *Vglut3*^{KO} IHCs is unknown. Therefore, to ask whether voltage-gated Ca^{2+} channels cluster with ribbons in *Vglut3*^{KO} IHCs, we immunolabeled $Ca_V1.3$ with CtBP2 and GluA3. As in unexposed *Vglut3*^{WT} and *Vglut3*$^{+/-}$ IHCs, $Ca_V1.3$ channels were located between presynaptic ribbons and postsynaptic AMPA receptors in unexposed *Vglut3*^{KO} IHCs (Fig. 6*A*,*B*). Next, we checked for noise-induced synapse loss during the noise exposure.

As reported above in Figure 4, in *Vglut3*^{KO}, noise exposure did not result in loss of IHC ribbon synapse number at 1 d or 2 weeks after exposure (Table 2). Previous experiments in CBA/CaJ^{WT} mice showed that loss of synaptic elements was nearly complete immediately after a 2 h exposure (Liberman et al., 2015). Thus, to check for immediate synapse loss in the IHC region that may have been repaired or cleared of debris by 1 d after exposure, we looked at 0 h after 2 h of 100 dB SPL exposure. Some *Vglut3*^{WT} and *Vglut3*$^{+/-}$ synapses were already disintegrated after 2 h of noise exposure (Fig. 6*C*,*E*). While Figure 6 shows representative images from *Vglut3*$^{+/-}$, we made similar observations in *Vglut3*^{WT}. We observed presynaptic ribbons with $Ca_V1.3$ that lacked postsynaptic GluA3 (Fig. 6C_1), and we observed lone $Ca_V1.3$ clusters lacking both the ribbon and GluA3 (Fig. 6C_2). These observations are consistent with previous experiments in CBA/CaJ^{WT} mice that showed either loss of synaptic elements or downregulation of AMPA receptors immediately after noise trauma (Liberman et al., 2015). In contrast, *Vglut3*^{KO} synapses appeared intact (Fig. 6*D*,*F*). Postsynaptic GluA3 remained juxtaposed to the presynaptic elements. The presynaptic active zone, defined by a ribbon and $Ca_V1.3$, appeared to remain intact in *Vglut3*^{KO} IHCs, suggesting that presynaptic Ca^{2+} influx alone was insufficient to disassemble the active zone.

Recovery of cochlear function in *Vglut3* mice after 94 dB exposure

Physiological and anatomical assessments following the 100 dB SPL exposure demonstrated better recovery of ABR threshold and synapse number in *Vglut3*^{WT} mice relative to *Vglut3*$^{+/-}$ mice (Figs. 1*C*, 4*B*,*C*; Tables 1, 2). We wondered whether the improved recovery of hearing function in *Vglut3*^{WT} relative to *Vglut3*$^{+/-}$ would generalize to other levels of exposure. Exposures >100 dB for 2 h are expected to cause irreversible damage to cochlear cells, including the outer hair cells, which might occlude observation of functional recovery due to synapse regeneration (Wang et al., 2002). Therefore, to further investigate this phenomenon, we reduced the exposure level to 94 dB SPL and assessed hearing function by ABR and DPOAE before exposure, and at 1 d, 2 weeks, and 4 weeks after exposure.

For the four assessment times, there were no significant differences in ABR thresholds between *Vglut3*^{WT} and *Vglut3*$^{+/-}$ mice at any test frequency (Fig. 7*A*; mixed-model ANOVA, $p = 0.98$). The persistent elevation of ABR thresholds at 32, 45.2, and 64 kHz was most likely due to aging on the C57BL/6J background, as suggested by our assessment of aging in unexposed control mice in Figure 8 (bottom). Thus, 2 h of 94 dB SPL exposure caused ABR threshold shifts at 1 d that appeared to recover to control levels by 2 and 4 weeks after exposure in *Vglut3*^{WT} and *Vglut3*$^{+/-}$ mice (Fig. 7*A*).

The amplitude of ABR wave I reflects the number of ANFs simultaneously activated at sound onset, which depends on the number of intact and active IHC-ANF synapses. Figure 7*B–D* shows that the amplitude of ABR wave I tended to recover faster in *Vglut3*^{WT} than *Vglut3*$^{+/-}$ following the 94 dB SPL exposure. For the 22.6 kHz tone, in response to all stimulus levels (20–85 dB SPL), ABR wave I amplitudes were reduced at 1 d after exposure relative to amplitudes in unexposed mice for *Vglut3*^{WT} and *Vglut3*$^{+/-}$ (Fig. 7*B*). In *Vglut3*^{WT} mice, by 2 weeks after exposure, wave I amplitudes were significantly different from unexposed mice for only two of the input levels (40 and 85 dB SPL); by 4 weeks after exposure, only the response to the 20 dB SPL tone level was significantly different from the responses of unexposed ears (Dunnett's *post hoc* test, $p < 0.05$). In contrast, *Vglut3*$^{+/-}$ mice exhibited significantly reduced wave I response amplitudes relative to unexposed controls for 13 of the 15 probe levels at 2

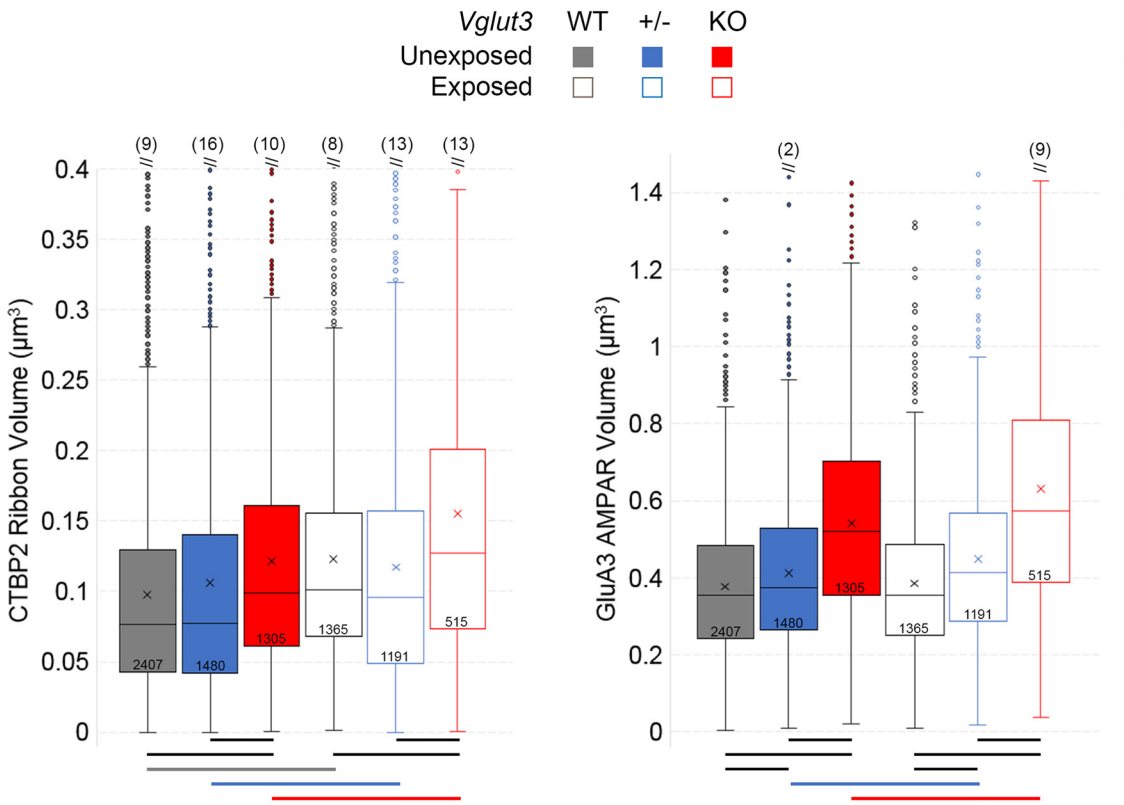

Figure 5. Ribbon synapses are larger after noise and without Vglut3. CtBP2 volumes (left) or GluA3 volumes (right) for paired synapses of midcochlear IHCs (35 kHz location) in $Vglut3^{WT}$, $Vglut3^{+/-}$, and $Vglut3^{KO}$ before and 2 weeks after 100 dB exposure. Tukey's box-and-whiskers: box shows the second quartile (or interquartile range) with median (horizontal line), mean (X), and number of synapses per group (e.g., $n = 2407$ for unexposed WT); whiskers extend down to minimum and upward for 1.5 × the interquartile range. Outliers are shown as individual points; number of outliers off scale are quantified in parentheses. Bottom, Horizontal bars represent significant differences in the distribution of data between groups (Kolmogorov–Smirnov test, $p < 0.05$; for exact p values and effect size estimates, see Table 4). Six groups: $N = 3–6$ cochleae per group; 8–13 images per group; 1305–2407 synapses per group.

Table 4. Ribbon or GluA3 volume per synapse (μm^3, all paired synapses) for unexposed or 2 weeks after 100 dB SPL exposure in midcochlea of $Vglut3^{WT}$, $Vglut3^{+/-}$, or $Vglut3^{KO}$[a]

	Unexposed		2 weeks		
Genotype	Mean ± SD	Median	Mean ± SD	Median	Kolmogorov–Smirnov test exposure
Ribbons					
$Vglut3^{WT}$	0.098 ± 0.079	0.076	0.123 ± 0.08	0.101	$p = 9e-33$ (0.3)*
$Vglut3^{+/-}$	0.106 ± 0.095	0.078	0.117 ± 0.092	0.096	$p = 2e-7$ (0.2)*
$Vglut3^{KO}$	0.122 ± 0.088	0.099	0.155 ± 0.116	0.127	$p = 2e-8$ (0.3)*
Kolmogorov–Smirnov test WT ±	$p = 0.2$		$p = 5e-12$ (0.1)		
Kolmogorov–Smirnov test WT KO	$p = 2e-17$ (0.3)*		$p = 3e-8$ (0.3)*		
GluA3					
$Vglut3^{WT}$	0.377 ± 0.182	0.355	0.385 ± 0.188	0.354	$p = 0.3$
$Vglut3^{+/-}$	0.413 ± 0.209	0.374	0.448 ± 0.225	0.414	$p = 2e-4$ (0.2)*
$Vglut3^{KO}$	0.542 ± 0.259	0.52	0.63 ± 0.342	0.575	$p = 4e-4$ (0.2)*
Kolmogorov–Smirnov test WT ±	$p = 1e-4$ (0.1)		$p = 3e-10$ (0.3)*		
Kolmogorov–Smirnov test WT KO	$p = 6e-73$ (0.8)*		$p = 5e-50$ (0.9)*		

[a]Values are number of animals-images-synapses unexposed: WT, 4-12-2407; HET, 3-8-1480; KO, 6-13-1305. Number of animals-images-synapses 2 weeks after exposure: WT, 3-8-1365; HET, 4-10-1191; KO, 3-6-515. p value (effect size; Kolmogorov–Smirnov test).

*Comparisons with p values < 0.05 and effect size ≥ 0.2.

weeks after exposure, and still for 7 of the 15 levels by 4 weeks after exposure (Dunnett's *post hoc* test, $p < 0.05$). Relative to $Vglut3^{WT}$ at 4 weeks after exposure, $Vglut3^{+/-}$ mice had significantly reduced ABR wave I amplitudes at 9 of the 15 input levels (Wilcoxon rank sum test: 30 dB, $p = 0.0074$; 35 dB, $p = 0.0019$; 40 dB, $p = 0.0391$; 45 dB, $p = 0.0083$; 50 dB, $p = 0.025$; 60 dB, $p = 0.0295$; 75 dB, $p = 0.0479$; 80 dB, $p = 0.0176$; 85 dB, $p = 0.0348$). For example, in response to 22.6 kHz tones at 85 dB SPL, the ABR wave I amplitude in $Vglut3^{WT}$ mice was on average ~27% larger compared with $Vglut3^{+/-}$ mice at 4 weeks after (Fig. 7*C*,*D*). By comparison, for the 8 kHz tone, which probes the less affected apical cochlea, the ABR wave I amplitudes of $Vglut3^{WT}$ and $Vglut3^{+/-}$ did not diverge over time after exposure.

Age-related hearing loss in $Vglut3^{WT}$ and $Vglut3^{+/-}$ mice

Above, we noise-exposed mice on C57BL/6J background at 9–11 weeks of age. This background strain begins to show progressive high-frequency hearing loss in the ensuing months. To interpret

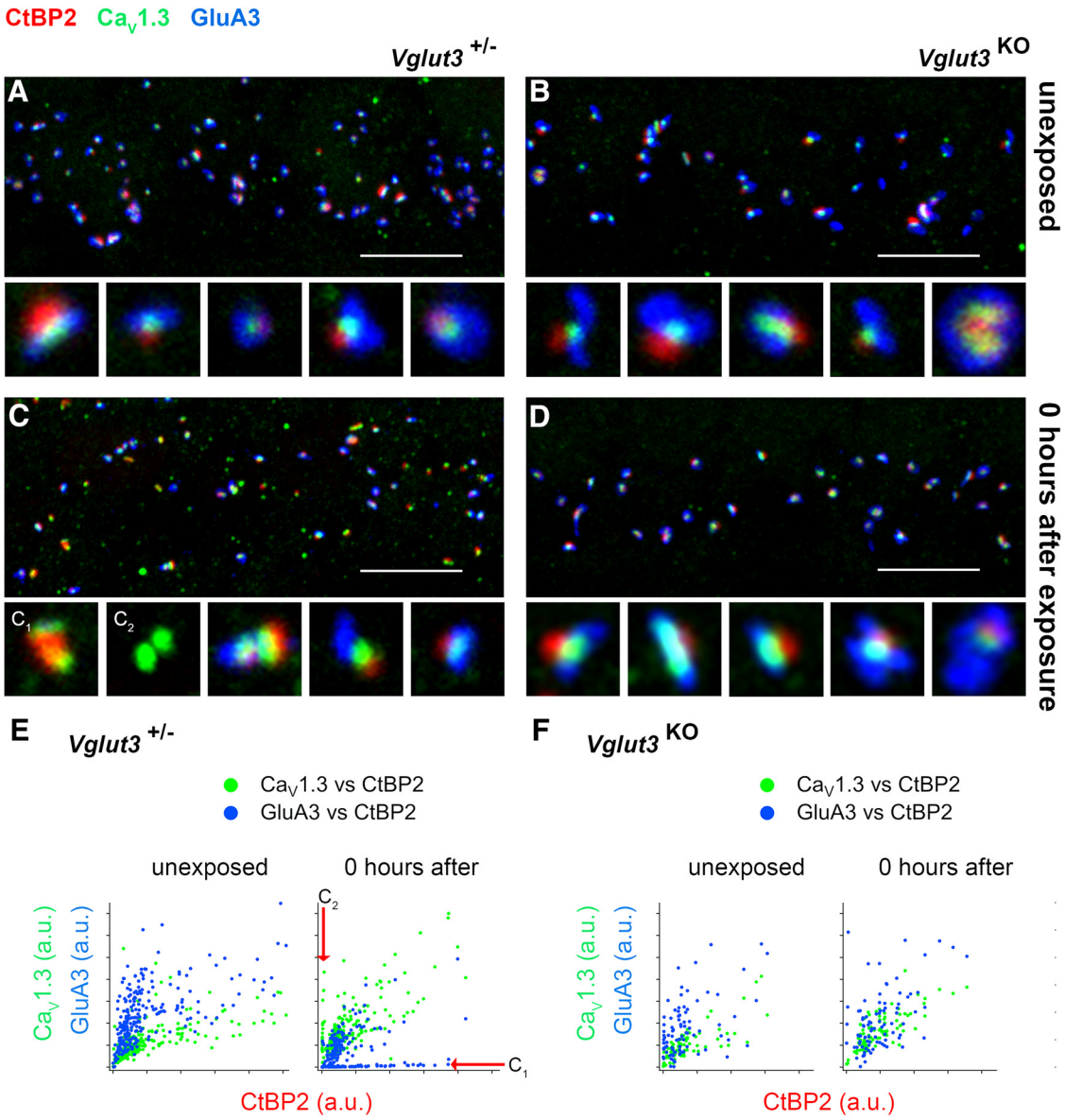

Figure 6. *Vglut3*^{KO} IHCs cluster voltage-gated Ca^{2+} channels with ribbons; synapses are not lost after noise. ***A***, Unexposed *Vglut3*$^{+/-}$. Presynaptic voltage-gated Ca^{2+} channels are labeled with anti-$Ca_V1.3$; presynaptic ribbons with anti-CtBP2; and postsynaptic AMPA receptors with anti-GluA3. Scale bar, 5 μm. Bottom, Small boxes are 1 μm × 1 μm. ***B***, Unexposed *Vglut3*^{KO}. ***C***, *Vglut3*$^{+/-}$ immediately after 2 h of 100 dB noise exposure. ***D***, *Vglut3*^{KO} immediately after 2 h of 100 dB noise exposure. Each image is from the 35 kHz region. ***E***, *Vglut3*$^{+/-}$ unexposed (left) or 0 h after exposure (right). For each synapse, the intensity of $Ca_V1.3$ (green markers) and GluA3 (blue markers) is plotted as a function of CtBP2 intensity (a.u., arbitrary units of pixel intensity). Red horizontal arrow indicates ribbon synapses having GluA3 immunofluorescence near 0 a.u. (blue markers along the abscissa) (e.g., see C_1). Green markers along the ordinate represent synapses with near 0 CtBP2 and, typically, near 0 GluA3 such that only $Ca_V1.3$ remains (red vertical arrow) (e.g., see C_2). ***F***, *Vglut3*^{KO} unexposed (left) or 0 h after exposure (right).

the recovery of hearing function after noise exposure in *Vglut3*^{WT} and *Vglut3*$^{+/-}$ mice (Figs. 1, 7), we asked whether age-related hearing loss differed between the two genotypes in unexposed mice. Between 2 and 3 months of age, ABR threshold shifts were observed only for the highest frequencies (Fig. 8). By 4–6 months, there were threshold elevations for middle and high frequencies; by 9 months, for all 8 test frequencies. The progressive high-frequency threshold shifts presumably reflect the effects of the $Cdh23^{753A}$ allele known to be present on the C57BL/6J background (Noben-Trauth et al., 2003). Unexposed *Vglut3*$^{+/-}$ mice demonstrated similar age-related hearing loss as seen in *Vglut3*^{WT} mice. The assessment in Figure 7*A* shows a persistent threshold shift at 4 weeks after 94 dB exposure for the highest frequencies, similar to the shifts seen between 2–3 or 3–4 months in Figure 8 due to aging.

Outer hair cell function in *Vglut3* mice after 94 or 100 dB exposure

The hallmark of synaptopathic noise exposure is destruction of some synapses while the inner and outer hair cells themselves survive. However, sublethal effects of noise on outer hair cells can affect cochlear function. Low-level cochlear vibrations are amplified by active processes in the outer hair cells that exert forces to counteract viscous dampening in the fluid-filled inner ear (Fisher et al., 2012). This mechanical positive feedback increases hearing sensitivity and enhances frequency selectivity by affecting the excitation of IHCs, which release glutamate onto ANFs at the ribbon synapses. Hearing thresholds thus depend on cochlear amplification by the outer hair cells, which can be damaged by noise exposure.

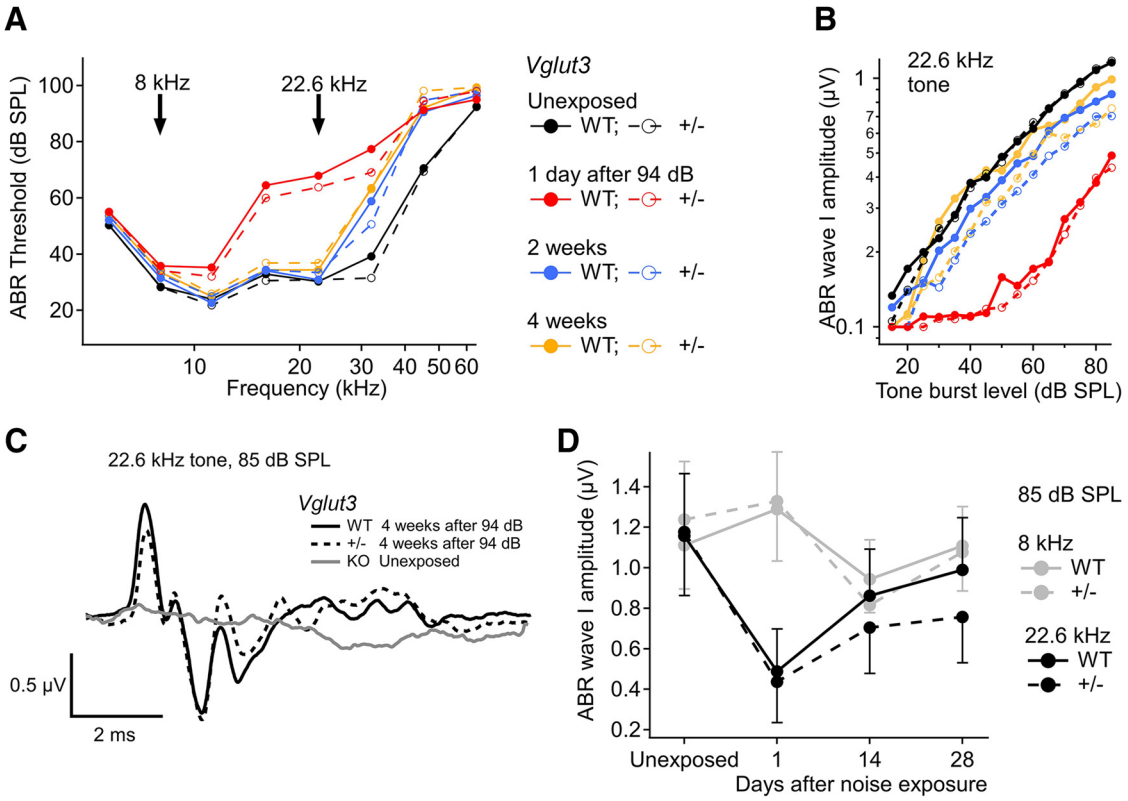

Figure 7. Better recovery of ABR wave I in *Vglut3*^{WT} than *Vglut3*$^{+/-}$ after 94 dB exposure. ***A***, Mean ABR thresholds in unexposed mice and following 94 dB exposure at 1 d, 2 weeks, and 4 weeks. Eight groups (genotype × time); $N = 16–19$ animals per group. Legend applies also to ***B***. ***B***, Mean ABR wave I amplitudes versus tone burst level for the same mice in ***A***. ***C***, ABR average waveforms (5 mice per genotype) in response to 85 dB SPL tone pips at 22.6 kHz at 4 weeks after exposure for *Vglut3*^{WT} and *Vglut3*$^{+/-}$, and in unexposed *Vglut3*^{KO} mice that showed a measurable response. ***D***, ABR wave I amplitude (mean ± SD) over time after 94 dB exposure in *Vglut3*^{WT} ($N = 10$) and *Vglut3*$^{+/-}$ ($N = 8$) for the 8 kHz and 22.6 kHz probe tones.

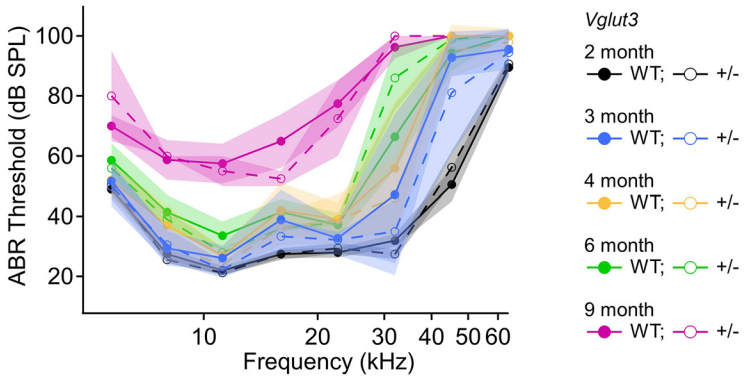

Figure 8. Age-related threshold shifts are similar in C57BL/6J *Vglut3*^{WT} and *Vglut3*$^{+/-}$ mice. ABR threshold shifts from 2 to 9 months demonstrate the well-known progressive hearing loss of the background strain, beginning at the highest frequencies, in *Vglut3*^{WT} and *Vglut3*$^{+/-}$ mice. Ten groups (age × genotype). Data are mean ± SD; $N = 2–10$ animals per group.

To control for outer hair cell effects that might differ by genotype, we measured DPOAE levels as a reflection of cochlear function and outer hair cell integrity over time in unexposed mice and after 94 or 100 dB SPL exposure. Figure 9*A*, *B* shows group mean emission levels as a function of frequency (f_2) before, 1 d, and 28 d after exposure to 94 or 100 dB SPL. *Vglut3*^{WT}, *Vglut3*$^{+/-}$, and *Vglut3*^{KO} mice had similar DPOAE response profiles in unexposed ears, although some cohorts of *Vglut3*^{KO} mice tended to have smaller emissions levels at the highest frequencies only (Fig. 9*A*,*B*, left). Figure 9*C–E* shows the group means of the mean emission levels across all frequencies for the 3 groups over time (Fig. 9*C*: unexposed; Fig. 9*D*: 94 dB SPL; Fig. 9*E*: 100 dB SPL). Comparing genotypes at each time, unexposed mice had similar DPOAE levels (Fig. 9*C*; two-tailed *t* test with Bonferroni correction, not significant for all four times, $p = 0.02–0.68$). Within each genotype in the unexposed group, DPOAE levels did not change significantly over the 1 month period after the initial test at 9–11 weeks of age (Fig. 9*C*; $p = 0.06–0.53$).

One day after exposure to 8-16 kHz noise at 94 or 100 dB SPL, DPOAE levels in exposed ears were depressed relative to unexposed *Vglut3*^{WT}, *Vglut3*$^{+/-}$, and *Vglut3*^{KO} mice (Fig. 9*A*,*B*, middle, *D*,*E*; $p = 1e^{-6}$ to $1e^{-17}$). For the 100 dB exposure, at 1 d, the *Vglut3*^{WT} emissions levels were significantly larger than *Vglut3*$^{+/-}$ or *Vglut3*^{KO} (Fig. 9*E*; wt > het, $p = 1e^{-9}$; WT > KO, $p < 1e^{-6}$). Two and 4 weeks after the 94 dB exposure, DPOAE levels remained significantly depressed relative to unexposed levels in *Vglut3*^{KO} ($p < 1e^{-4}$), whereas *Vglut3*^{WT} and *Vglut3*$^{+/-}$ were not significantly different from unexposed levels at 2 and 4 weeks, respectively (Fig. 9*D*; $p = 0.13$ and $p = 0.0065$). Two and 4 weeks after the 100 dB exposure, DPOAE levels remained significantly smaller than unexposed levels for all genotypes (Fig. 9*E*; $p = 0.003–4.2e^{-8}$). By 4 weeks after exposure (Fig. 9*A*,*B*, right), there were no significant differences between genotypes for either exposure (Fig. 9*D*,*E*; $p = 0.03–0.67$).

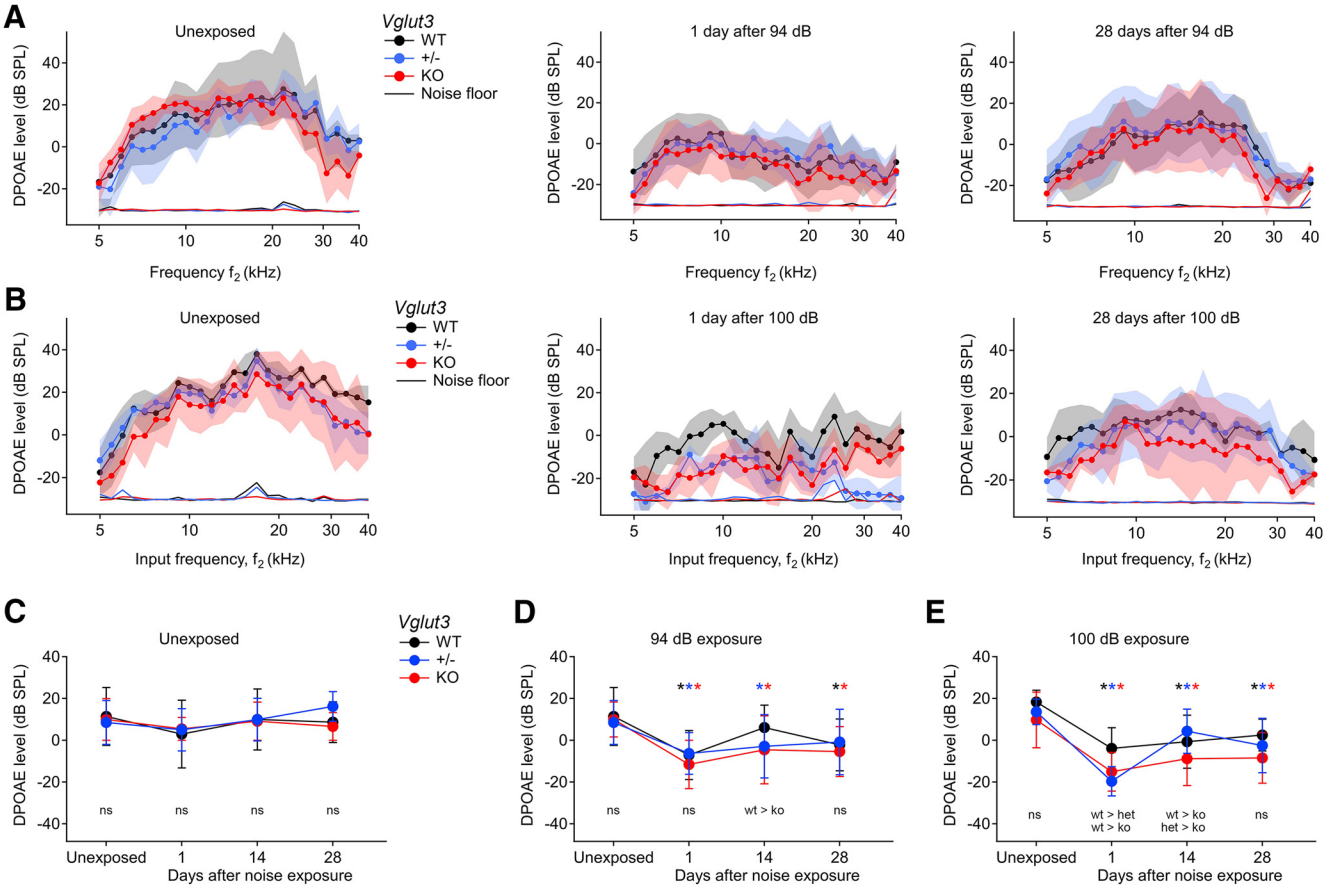

Figure 9. DPOAE levels were reduced in *Vglut3*^{WT}, *Vglut3*$^{+/-}$, and *Vglut3*^{KO} mice after 94 or 100 dB exposure. ***A***, ***B***, DPOAE levels (mean ± SD) as a function of input frequency (f_2) in unexposed mice (left), 1 d after (middle), or 28 d after (right) 94 dB exposure (***A***) or 100 dB exposure (***B***) to 8–16 kHz octave-band noise for 2 h. ***C–E***, DPOAE levels (mean ± SD) over time in unexposed mice (***C***), and in mice exposed to 94 dB (***D***) or 100 dB SPL noise (***E***). For each group (genotype × exposure condition), the mean DPOAE level across all frequencies per mouse was used to calculate the group means. $N = 4–13$ mice per group, exposed at 9–11 weeks of age. Bottom markers, Statistical comparison between three genotypes for each exposure condition (dB SPL group × time after exposure). Top markers, Statistical comparison of genotype over time within each dB SPL group. The color of the asterisks at each time indicates the genotypes having significantly smaller mean DPOAE levels relative to unexposed.

Discussion

Glutamate is required for noise-induced cochlear synaptopathy, but the mechanism is unknown

To directly test the idea that glutamate is required for noise-induced cochlear excitotoxicity, we exposed *Vglut3*^{KO} mice to synaptopathic noise. We found that genetic removal of Vglut3 prevented noise-induced loss of synapse number (Fig. 4). The Vgluts are specific for glutamate, unable to transport the similar amino acids and potential neurotransmitters aspartate, glutamine, or GABA (Schäfer et al., 2002). Therefore, as has been presumed based on previous pharmacological studies *in vivo* and in cell culture (Puel et al., 1994; Wang and Green, 2011), we now can conclude with little doubt that noise-induced cochlear excitotoxicity requires synaptic release of glutamate from IHCs.

The mechanism(s) of glutamate-dependent cochlear excitotoxicity remain unclear but likely involve postsynaptic Ca^{2+}. Although they have yet to be directly demonstrated functionally in mammalian ANFs, the existence of Ca^{2+}-permeable AMPA receptors at hair cell synapses appears to be evolutionarily conserved in fish, frogs, and mammals (Sebe et al., 2017). Postsynaptic Ca^{2+} influx through AMPA, kainate, or NMDA receptors, or through voltage-gated Ca^{2+} channels may activate calpain-mediated cell death (Chen et al., 2009). On the other hand, postsynaptic Ca^{2+} influx may protect synapses by triggering rapid removal of AMPA receptors via endocytosis during exposure to loud sounds (Chen et al., 2007). Furthermore, glutamatergic activity that is damaging in one context may be beneficial in another. For example, Ca^{2+} influx through NMDA receptors may be required for synapse regeneration after trauma (d'Aldin et al., 1997).

Glutamate regulates presynaptic and postsynaptic size

IHCs require Vglut3 for quantal transmission and normal ANF activity. As in hair cells of the lateral line organ (Obholzer et al., 2008), Vglut1 and Vglut2 do not compensate in the absence of Vglut3. Despite the lack of glutamatergic transmission, at 9–11 weeks of age, approximately half the normal number of synapses are maintained as AMPA receptors juxtaposed to presynaptic ribbons (Figs. 2, 4). Interestingly, these postsynaptic arrays of AMPA receptors in *Vglut3*^{KO} mice were significantly larger than *Vglut3*^{WT} or *Vglut3*$^{+/-}$ (Fig. 5). AMPA receptor endocytosis triggered by application of AMPA or NMDA in cell culture depends on Ca^{2+} influx and is inhibited by blocking voltage-gated Ca^{2+} channels (Chen et al., 2009). We propose that lack of glutamate-induced Ca^{2+} influx reduced AMPA receptor endocytosis in *Vglut3*^{KO}, resulting in enlargement of the array of AMPA receptors labeled by anti-GluA3. Additionally, we observed larger presynaptic ribbons in *Vglut3*^{KO} mice (Fig. 5), reminiscent of observations in WT animals showing that larger ribbons belong

to less active synapses (Merchan-Perez and Liberman, 1996; Sheets et al., 2012; Nicolson, 2015).

Ribbon synapses regenerate following an initial loss with acoustic trauma in C57BL/6J

After an initial loss of ~50% of synapses with acoustic trauma, we found that approximately half of those synapses regenerated spontaneously in $Vglut3^{WT}$ (Figs. 3, 4). This contrasts with the conventional view based on experiments in CBA/CaJ^{WT} mice showing that ribbon synapse loss is permanent. Regeneration of synapses after noise exposure, or lack thereof, may depend on the animal species, experimental conditions, or the actions of neurotrophic factors (Kujawa and Liberman, 2009; Shi et al., 2013; Wan et al., 2014; Chen et al., 2018). Although it does not imply causality, we found that recovery of IHC ribbon synapse number was correlated with recovery of ABR threshold after the 100 dB exposure (Figs. 1, 4). We found that the enhancement of recovery in $Vglut3^{WT}$ was not readily explained by differences in DPOAE or age-related hearing loss (Figs. 8, 9).

Two copies of *Vglut3* are better than one

Significantly fewer synapses regenerated in $Vglut3^{+/-}$ than $Vglut3^{WT}$ after 100 dB exposure, suggesting a role for Vglut3 in regeneration. $Vglut3^{+/-}$ mice also had poorer recovery of ABR wave I amplitudes after the 94 dB exposure, suggesting a reduction in Vglut3 function detectable when the system is challenged. These phenotypes may result from reduction of glutamate secretion during the recovery period (d'Aldin et al., 1997), if $Vglut3^{WT}$ IHCs release more glutamate than $Vglut3^{+/-}$ IHCs after noise trauma. We found no other indirect evidence suggesting increased release of glutamate from $Vglut3^{WT}$ IHCs: Upon noise exposure, $Vglut3^{+/-}$ mice lose synapses, such as $Vglut3^{WT}$ (Fig. 4). In unexposed $Vglut3^{+/-}$ mice, just one copy of *Vglut3* was sufficient to maintain normal auditory thresholds, synapse numbers, and wave I amplitudes (Figs. 1, 4, 7). Perhaps more demanding auditory stimuli requiring more Vglut3 activity would reveal fatigue in $Vglut3^{+/-}$. Another possibility is that the $Vglut3^{+/-}$ haplo-insufficiency relates to reduced binding interactions of Vglut3 with other proteins that support regeneration.

Glutamate-independent effects of noise on the IHC-ANF synapse

Electron micrographs and immunohistofluorescence have been used to illustrate presynaptic loss and sublethal damage to the IHC that accompanies ANF terminal swelling and vacuolization (Robertson, 1983; Kujawa and Liberman, 2009). Like postsynaptic Ca^{2+} overload in the ANF, presynaptic Ca^{2+} overload may damage the IHC. In $Vglut3^{WT}$ and $Vglut3^{+/-}$ IHCs, noise exposure resulted in unpairing of some CtBP2 and $Ca_V1.3$ puncta (Fig. 6*A*,*C*,*E*). In $Vglut3^{KO}$ IHCs, the proper localization of $Ca_V1.3$ and the lack of unpairing suggest that active-zone destruction follows glutamate release, and that noise-induced presynaptic Ca^{2+} influx is insufficient for synaptic disintegration (Fig. 6*B*,*D*,*F*).

Unexpectedly, 2 weeks after exposure, we found that $Vglut3^{KO}$ ribbons and AMPA receptors were significantly different in volume than unexposed $Vglut3^{KO}$ (Fig. 5), suggesting noise-induced changes that were independent of glutamate. In $Vglut3^{WT}$ and $Vglut3^{+/-}$ as well, ribbons appeared to be embiggened by 2 weeks after noise. GluA3 puncta in $Vglut3^{+/-}$ appeared to become larger by 2 weeks after noise, but less so than $Vglut3^{KO}$, and in $Vglut3^{WT}$ the size of GluA3 puncta was maintained after noise (Fig. 5). We propose a bidirectional control of AMPA receptor number and thus postsynaptic size in which glutamate acts to reduce, and other releasable factors act to increase, AMPA receptor number. In the absence of glutamate release, synaptic activity results in larger synapses.

Our results show that protons and other chemical constituents of synaptic vesicles, such as aspartate, adenosine, and proinflammatory cytokines, if present, are insufficient to cause noise-induced loss of IHC-ANF synapse number. However, this does not exclude the possible involvement of other released substances in glutamate-dependent or -independent mechanisms. Indeed, Vglut3 is identified mainly in neurons coexpressing neurotransmitter transporters for GABA, acetylcholine, or serotonin (El Mestikawy et al., 2011). However, corelease of neurotransmitter from hair cells is unknown. Additionally, synaptic vesicles are acidified, and acidosis may contribute to ANF excitotoxicity or plasticity through activation of the excitatory acid-sensing ion channel-2 in mice (Peng et al., 2004). Indeed, hair cell synapses of the frog amphibian papilla are known to acidify the synaptic cleft by releasing protons, as demonstrated by transient inhibition of the presynaptic Ca^{2+} current (Cho and von Gersdorff, 2014). If vesicular protons are a component of synaptic transmission, then a proton-mediated EPSC is expected; however, application of the AMPA receptor antagonist CNQX completely blocks the EPSC in mammalian ANFs (Glowatzki and Fuchs, 2002), suggesting that protons are not acting as neurotransmitters.

Type I ANF subtype identity in $Vglut3^{KO}$ mice

Type I ANFs (also called Type I spiral ganglion neurons) differentiate into subtypes in an activity-dependent developmental progression. In the absence of glutamatergic activity, they develop into less-diverse intermediate subtype(s) based on single-cell RNA sequencing (Shrestha et al., 2018; Sun et al., 2018). It is possible that ANFs in $Vglut3^{KO}$ fail to diversify into the more excitotoxically vulnerable phenotypes. If synapses belonging to the more vulnerable ANFs are already absent in $Vglut3^{KO}$, because they failed to differentiate or they already died off, then it remains a possibility they could be damaged by glutamate-independent processes in $Vglut3^{WT}$. Resolution of the requirement for glutamate in excitotoxicity of high- versus medium- and low-spontaneous-rate ANFs will require a conditional $Vglut3^{KO}$ mouse that develops the normal diversified set of ANFs before induction of deafness, followed by noise exposure.

More work is needed to understand the contributions of presynaptic, postsynaptic, efferent, and spike-generator mechanisms to ANF activity under different conditions and in different species (Ohlemiller et al., 2016; Reijntjes and Pyott, 2016). There remain unanswered questions about the influence of IHC-driven activity on ANF identity. Interestingly, spontaneous activity persists in the developing $Vglut3^{KO}$ cochlea, and the intrinsic excitability of ANFs is enhanced (Babola et al., 2018). There is not a simple phenotypic match between the ANFs remaining in adult $Vglut3^{KO}$ (remaining in the absence of glutamate) and those in $Vglut3^{WT}$ that develop normally into a more excitotoxically resistant subtype (i.e., those that remain after the noise-induced glutamate exposure). For example, synaptic ribbon enlargement in $Vglut3^{KO}$ (Fig. 5) is contrary to the synaptic phenotype of the ANFs in $Vglut3^{WT}$ that are thought to be more resistant, which have smaller ribbons. We note that the correlation between excitotoxic vulnerability, spontaneous spike rate, and threshold in cat and guinea pig has not been demonstrated in mouse

(Merchan-Perez and Liberman, 1996; Furman et al., 2013). It is crucial for future experiments to directly demonstrate the relationships between genetically defined Type I ANF subtypes and physiologically defined ANF phenotypes (Petitpré et al., 2018).

References

Akil O, Seal RP, Burke K, Wang C, Alemi A, During M, Edwards RH, Lustig LR (2012) Restoration of hearing in the VGLUT3 knockout mouse using virally mediated gene therapy. Neuron 75:283–293.

Babola TA, Li S, Gribizis A, Lee BJ, Issa JB, Wang HC, Crair MC, Bergles DE (2018) Homeostatic control of spontaneous activity in the developing auditory system. Neuron 99:511–524.e5.

Chen H, Xing Y, Xia L, Chen Z, Yin S, Wang J (2018) AAV-mediated NT-3 overexpression protects cochleae against noise-induced synaptopathy. Gene Ther 25:251–259.

Chen Z, Kujawa SG, Sewell WF (2007) Auditory sensitivity regulation via rapid changes in expression of surface AMPA receptors. Nat Neurosci 10:1238–1240.

Chen Z, Peppi M, Kujawa SG, Sewell WF (2009) Regulated expression of surface AMPA receptors reduces excitotoxicity in auditory neurons. J Neurophysiol 102:1152–1159.

Cho S, von Gersdorff H (2014) Proton-mediated block of Ca^{2+} channels during multivesicular release regulates short-term plasticity at an auditory hair cell synapse. J Neurosci 34:15877–15887.

d'Aldin CG, Ruel J, Assié R, Pujol R, Puel JL (1997) Implication of NMDA type glutamate receptors in neural regeneration and neoformation of synapses after excitotoxic injury in the guinea pig cochlea. Int J Dev Neurosci 15:619–629.

Elberling C, Don M (1987) Threshold characteristics of the human auditory brain stem response. J Acoust Soc Am: 81:115–121.

El Mestikawy S, Wallén-Mackenzie A, Fortin GM, Descarries L, Trudeau LE (2011) From glutamate co-release to vesicular synergy: vesicular glutamate transporters. Nat Rev Neurosci 12:204–216.

Eybalin M, Caicedo A, Renard N, Ruel J, Puel JL (2004) Transient Ca^{2+}-permeable AMPA receptors in postnatal rat primary auditory neurons. Eur J Neurosci 20:2981–2989.

Fisher JA, Nin F, Reichenbach T, Uthaiah RC, Hudspeth AJ (2012) The spatial pattern of cochlear amplification. Neuron: 76:989–997.

Furman AC, Kujawa SG, Liberman MC (2013) Noise-induced cochlear neuropathy is selective for fibers with low spontaneous rates. J Neurophysiol 110:577–586.

Glowatzki E, Fuchs PA (2002) Transmitter release at the hair cell ribbon synapse. Nat Neurosci 5:147–154.

Greene CC, McMillan PM, Barker SE, Kurnool P, Lomax MI, Burmeister M, Lesperance MM (2001) DFNA25, a novel locus for dominant nonsyndromic hereditary hearing impairment, maps to 12q21–24. Am J Hum Genet 68:254–260.

Hirose K, Discolo CM, Keasler JR, Ransohoff R (2005) Mononuclear phagocytes migrate into the murine cochlea after acoustic trauma. J Comp Neurol 489:180–194.

Jäger W, Goiny M, Herrera-Marschitz M, Flock A, Hökfelt T, Brundin L (1998) Sound-evoked efflux of excitatory amino acids in the guinea-pig cochlea in vitro. Exp Brain Res 121:425–432.

Jing Z, Rutherford MA, Takago H, Frank T, Fejtova A, Khimich D, Moser T, Strenzke N (2013) Disruption of the presynaptic cytomatrix protein bassoon degrades ribbon anchorage, multiquantal release, and sound encoding at the hair cell afferent synapse. J Neurosci 33:4456–4467.

Kujawa SG, Liberman MC (2009) Adding insult to injury: cochlear nerve degeneration after "temporary" noise-induced hearing loss. J Neurosci 29:14077–14085.

Kurabi A, Beasley KA, Chang L, McCann J, Pak K, Ryan AF (2017) Peptides actively transported across the tympanic membrane: functional and structural properties. PLoS One 12:e0172158.

Lee C, Guinan JJ Jr, Rutherford MA, Kaf WA, Kennedy KM, Buchman CA, Salt AN, Lichtenhan JT (2019) Cochlear compound action potentials from high-level tone bursts originate from wide cochlear regions that are offset toward the most sensitive cochlear region. J Neurophysiol 121:1018–1033.

Liberman LD, Suzuki J, Liberman MC (2015) Dynamics of cochlear synaptopathy after acoustic overexposure. J Assoc Res Otolaryngol 16:205–219.

Littell RC, Henry PR, Ammerman CB (1998) Statistical analysis of repeated measures data using SAS procedures. J Anim Sci 76:1216–1231.

Longenecker RJ, Alghamdi F, Rosen MJ, Galazyuk AV (2016) Prepulse inhibition of the acoustic startle reflex vs. auditory brainstem response for hearing assessment. Hear Res 339:80–93.

Martinez-Dunst C, Michaels RL, Fuchs PA (1997) Release sites and calcium channels in hair cells of the chick's cochlea. J Neurosci 17:9133–9144.

Merchan-Perez A, Liberman MC (1996) Ultrastructural differences among afferent synapses on cochlear hair cells: correlations with spontaneous discharge rate. J Comp Neurol 371:208–221.

Müller M, von Hünerbein K, Hoidis S, Smolders JW (2005) A physiological place-frequency map of the cochlea in the CBA/J mouse. Hear Res 202:63–73.

Nicolson T (2015) Ribbon synapses in zebrafish hair cells. Hear Res 330:170–177.

Noben-Trauth K, Zheng QY, Johnson KR (2003) Association of cadherin 23 with polygenic inheritance and genetic modification of sensorineural hearing loss. Nat Genet 35:21–23.

Obholzer N, Wolfson S, Trapani JG, Mo W, Nechiporuk A, Busch-Nentwich E, Seiler C, Sidi S, Söllner C, Duncan RN, Boehland A, Nicolson T (2008) Vesicular glutamate transporter 3 is required for synaptic transmission in zebrafish hair cells. J Neurosci 28:2110–2118.

Ohlemiller KK, Jones SM, Johnson KR (2016) Application of mouse models to research in hearing and balance. J Assoc Res Otolaryngol 17:493–523.

Ohn TL, Rutherford MA, Jing Z, Jung S, Duque-Afonso CJ, Hoch G, Picher MM, Scharinger A, Strenzke N, Moser T (2016) Hair cells use active zones with different voltage dependence of Ca^{2+} influx to decompose sounds into complementary neural codes. Proc Natl Acad Sci U S A 113:E4716–E4725.

Peng BG, Ahmad S, Chen S, Chen P, Price MP, Lin X (2004) Acid-sensing ion channel 2 contributes a major component to acid-evoked excitatory responses in spiral ganglion neurons and plays a role in noise susceptibility of mice. J Neurosci 24:10167–10175.

Petitpré C, Wu H, Sharma A, Tokarska A, Fontanet P, Wang Y, Helmbacher F, Yackle K, Silberberg G, Hadjab S, Lallemend F (2018) Neuronal heterogeneity and stereotyped connectivity in the auditory afferent system. Nat Commun 9:3691.

Puel JL, Pujol R, Tribillac F, Ladrech S, Eybalin M (1994) Excitatory amino acid antagonists protect cochlear auditory neurons from excitotoxicity. J Comp Neurol 341:241–256.

Puel JL, Ruel J, d'Aldin CG, Pujol R (1998) Excitotoxicity and repair of cochlear synapses after noise-trauma induced hearing loss. Neuroreport 9:2109–2114.

Reijntjes DO, Pyott SJ (2016) The afferent signaling complex: regulation of Type I spiral ganglion neuron responses in the auditory periphery. Hear Res 336:1–16.

Robertson D (1983) Functional significance of dendritic swelling after loud sounds in the guinea pig cochlea. Hear Res 9:263–278.

Ruel J, Emery S, Nouvian R, Bersot T, Amilhon B, Van Rybroek JM, Rebillard G, Lenoir M, Eybalin M, Delprat B, Sivakumaran TA, Giros B, El Mestikawy S, Moser T, Smith RJ, Lesperance MM, Puel JL (2008) Impairment of SLC17A8 encoding vesicular glutamate transporter-3, VGLUT3, underlies nonsyndromic deafness DFNA25 and inner hair cell dysfunction in null mice. Am J Hum Genet 83:278–292.

Rutherford MA (2015) Resolving the structure of inner ear ribbon synapses with STED microscopy. Synapse 69:242–255.

Schäfer MK, Varoqui H, Defamie N, Weihe E, Erickson JD (2002) Molecular cloning and functional identification of mouse vesicular glutamate transporter 3 and its expression in subsets of novel excitatory neurons. J Biol Chem 277:50734–50748.

Seal RP, Akil O, Yi E, Weber CM, Grant L, Yoo J, Clause A, Kandler K, Noebels JL, Glowatzki E, Lustig LR, Edwards RH (2008) Sensorineural deafness and seizures in mice lacking vesicular glutamate transporter 3. Neuron 57:263–275.

Sebe JY, Cho S, Sheets L, Rutherford MA, von Gersdorff H, Raible DW (2017) Ca^{2+}-permeable AMPARs mediate glutamatergic transmission and excitotoxic damage at the hair cell ribbon synapse. J Neurosci 37:6162–6175.

Sheets L, Kindt KS, Nicolson T (2012) Presynaptic CaV1.3 channels regulate synaptic ribbon size and are required for synaptic maintenance in sensory hair cells. J Neurosci 32:17273–17286.

Shi L, Liu L, He T, Guo X, Yu Z, Yin S, Wang J (2013) Ribbon synapse plasticity in the cochleae of guinea pigs after noise-induced silent damage. PLoS ONE 8:e81566.

Shrestha BR, Chia C, Wu L, Kujawa SG, Liberman MC, Goodrich LV (2018) Sensory neuron diversity in the inner ear is shaped by activity. Cell 174:1229–1246.e17.

Sun S, Babola T, Pregernig G, So KS, Nguyen M, Su SM, Palermo AT, Bergles DE, Burns JC, Müller U (2018) Hair cell mechanotransduction regulates spontaneous activity and spiral ganglion subtype specification in the auditory system. Cell 174:1247–1263.e15.

Thirlwall AS, Brown DJ, McMillan PM, Barker SE, Lesperance MM (2003) Phenotypic characterization of hereditary hearing impairment linked to DFNA25. Arch Otolaryngol Head Neck Surg 129:830–835.

Wakabayashi S, Nakamura TY, Kobayashi S, Hisamitsu T (2010) Novel phorbol ester-binding motif mediates hormonal activation of Na^+/H^+ exchanger. J Biol Chem 285:26652–26661.

Wan G, Gómez-Casati ME, Gigliello AR, Liberman MC, Corfas G (2014) Neurotrophin-3 regulates ribbon synapse density in the cochlea and induces synapse regeneration after acoustic trauma. Elife 3:e03564.

Wang Q, Green SH (2011) Functional role of neurotrophin-3 in synapse regeneration by spiral ganglion neurons on inner hair cells after excitotoxic trauma in vitro. J Neurosci 31:7938–7949.

Wang Y, Hirose K, Liberman MC (2002) Dynamics of noise-induced cellular injury and repair in the mouse cochlea. J Assoc Res Otolaryngol 3:248–268.